Heliyon 10 (2024) e26926

Contents lists available at ScienceDirect

Heliyon

journal homepage: www.cell.com/heliyon

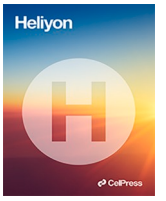

Research article

Optimizing 3D printed ankle-foot orthoses for patients with stroke: Importance of effective elastic modulus and finite element simulation

Chien-Hsien Yeh [a], Keng-Ren Lin [b], Fong-Chin Su [a,b], Hsiu-Yun Hsu [c,d], Li-Chieh Kuo [a,c,d], Chih-Chun Lin [e,*]

[a] Medical Device Innovation Center, National Cheng Kung University, Taiwan
[b] Department of Biomedical Engineering, National Cheng Kung University, Taiwan
[c] Department of Physical Medicine and Rehabilitation, National Cheng Kung University Hospital, National Cheng Kung University, Taiwan
[d] Department of Occupational Therapy, National Cheng Kung University, Taiwan
[e] Department of Physical Therapy, I-Shou University, Taiwan

ARTICLE INFO

Keywords:
Ankle-foot orthosis
3D printed materials
Finite element model
Effective elastic modulus

ABSTRACT

Patients with stroke often use ankle-foot orthoses (AFOs) for gait improvement. 3D printing technology has become a popular tool in recent years for the production of AFOs due to its strengths on customization and rapid manufacturing. However, the porosity of the 3D printed materials affects the kinetic features of these orthoses, leading to its lower-strength than solid ones. The effective elastic modulus of 3D printed material was measured following standard test method to obtain the kinetic features precisely in a finite element simulation. This study demonstrated that the porosity of 3D printed samples using 100% fill density was 11% for PLA and 16% for Nylon. As a result, their effective elastic modulus was reduced to 1/3 and 1/12 of fully solid objects, respectively, leading to a lower stiffness of 3D printed orthoses. A fatigue testing platform was built to verify our finite element model, and the findings of the fatigue test were consistent with the analysis of the finite element model. Further, our AFO has been proven to have a lifespan exceeding 200 thousand steps. Our study highlights the significance of determining the actual porosity of 3D printed samples by calculating the effective elastic modulus, which leads to a more precise finite element simulation and enables reliable prediction of the kinetic features of the AFO. Overall, this study provides valuable insights into the production and optimization of 3D printed AFOs for patients with stroke.

1. Introduction

Due to the neurological disorders caused by stroke, patients often experience a loss of muscle control in their lower limbs, resulting in drop foot during swing phase and inverted foot during stance phase. To compensate for the lack of momentum and energy needed for pushing off and lifting the foot, patients with stroke develop a circumduction gait [1]. Ankle-foot orthosis (AFO) is often used to correcting the gait of these patients, helping them improve their gait performance. Typically, AFOs are categorized into three main

* Corresponding author. No.1, Sec. 1, Syuecheng Rd, Dashu District, Kaohsiung City, 84001, Taiwan.
E-mail addresses: longerplus@gmail.com (C.-H. Yeh), krlin213@gmail.com (K.-R. Lin), fcsu@ncku.edu.tw (F.-C. Su), hyhsu@mail.ncku.edu.tw (H.-Y. Hsu), jkkuo@mail.ncku.edu.tw (L.-C. Kuo), chihchunlin@isu.edu.tw (C.-C. Lin).

https://doi.org/10.1016/j.heliyon.2024.e26926
Received 25 May 2023; Received in revised form 14 February 2024; Accepted 21 February 2024
Available online 27 February 2024

Abbreviations

AFOs	ankle-foot orthoses
Dtest	average density of material
Eref	elastic moduli of material
Etest	effective elastic modulus of material
FDM	fused deposition modeling
MT	material testing
PLA	polylactic acid
PoA	point of application
SLA	stereolithography apparatus
SLS	selective laser sintering
Vreal	solid volume
Vvoid	void volume
Vwhole	whole volume
West	estimated mass
Wreal	real mass of material
Wreal	real mass

types: anterior, posterior, and articulated. These AFO variants effectively address issues like drop foot and inversion foot, allowing patients to move about more freely in their daily lives [2]. In addition, powered AFOs such as the hydraulic ankle foot orthosis have also been developed [3]. However, these powered options can be more substantial in size and rely on batteries for functionality.

AFOs must be customized to fit the specific profiles of each patient's shank and foot, with therapists and related professionals typically using thermoplastic splint to create them. In recent years, 3D printing technology has been used to facilitate AFO development, primarily through the application of fused deposition modeling (FDM), selective laser sintering (SLS), and stereolithography apparatus (SLA). Mavroidis et al. [4] utilized the Viper SLA machine and the DSM Somos 9120 Epoxy to manufacture a posterior AFO in their study. Meanwhile, Walbran et al. [5] employed an SLS machine to sinter Nylon material and develop a posterior AFO with a carbon fiber composite joint. In another study, Scott et al. utilized an SLS machine and Nylon powders to create a posterior AFO equipped with two gas springs that could resist plantarflexion [6]. Schrank et al. [7] used an FDM machine and PC-ISO materials to fabricate a posterior AFO with an adjustable bending stiffness through strut size manipulation. It is worth noting that FDM is the predominant technology due to its fast production, low cost, and simple post-processing.

The strength of 3D printed components produced using FDM technology is typically lower than that of solid materials due to their high porosity and weakly connected structure [8]. The porosity is created between printing layers and their adjacent paths. If the fill density is 100%, it still may not ensure that the porosity is zero. Therefore, the finite element model of an FDM sample should not be taken as a solid material. Abbot et al. [9] have already proven that an error occurs in a finite element simulation if 3D printed samples are set as solid objects. So how do we set the material properties for 3D printed samples? Some finite element models have adopted effective mechanical properties, such as the effective elastic modulus or effective Poisson's ratio, for porous materials. The effective mechanical property represents the homogenized material property in the macroscale [10]. The effective mechanical properties are usually obtained from material testing using 3D printed specimens [8].

Some measuring platforms have been developed to observe the kinetic features of AFO. Lai et al. [11] developed an ankle–foot simulator to investigate the failure progression AFOs. The simulator integrated an automatic mechanism to mimic the gait cycle. Cha et al. [12] designed an AFO with shoelaces and tested its durability on a fatigue testing platform. The testing platform has round-shaped plastic dummies and outer rims to fix the AFO at the foot and shank portions. Their AFOs were tested for 300,000 cycles using a stretching force set to 50 N and a frequency of 1 Hz with sine waves. Bregman et al. [13] designed a bi-articular reciprocating universal compliance estimator to measure the angle and moment of the ankle and metatarsal-phalangeal joint. The estimator mechanism is simple, but the AFO motion was constrained to the sagittal plane. Some asymmetric AFOs, such as the commercial product ToeOFF (Allard Int.), may not be suitable for this measuring platform because the torsion relative to the longitudinal direction of the shank is ignored. Kobayashi et al. [14] used an automatic AFO stiffness measurement device to estimate the stiffness of an articulated AFO. The foot portion of the AFO moved with a rotary plate, and the shank portion of the AFO was fixed. This similar measuring platform also limited the AFO motion to the sagittal plane. The measuring platform should allow the limited deformation of AFO to match the real motion of the shank and foot, such as eversion, adduction, and abduction.

The ankle-foot simulator developed by Lai et al. has two degrees of freedom in the ankle joint, allowing for both plantar flexion/dorsiflexion and inversion/eversion movements [11]. Schrank et al. [7] also developed a stiffness testing device using a linear bearing to allow for deformation of the AFO along the longitudinal axis of the shank part. In order to compare the stiffness testing device with the ankle-foot simulator, Schrank et al. also disclosed a simpler measuring platform, which is more reliable for long-term testing such as fatigue testing, as there is a lower chance of needing to replace broken components.

In this study, our aim was to build a finite element model using the effective elastic modulus to obtain accurate kinetic features of the 3D printed AFO, such as load. The AFO was produced using the FDM process, with a fill density set at 100% for increased strength. The effective elastic modulus of the 3D printed components will be measured following the ASTM D638 standard (Standard Test

Method for Tensile Properties of Plastics) [15]. To verify the finite element model, we will build a fatigue testing platform and investigate the lifespan of our AFO. The jig mechanism of the fatigue testing platform must be simple and allow for deformation along the longitudinal axis of the shank, as well as allow for observation of torsion in asymmetric AFOs.

2. Methods

2.1. The 3D printed AFO and its finite element model

The AFO in this study is composed of a footplate, a joint part, and a strut (Fig. 1(a)). This is an asymmetric AFO, with the joint part and strut located only on the lateral side of the shank. The joint part was inserted a metal plate to enhance its stiffness. Except for the footplate, the strut and joint part are made of the 3D printed materials, Polylactic Acid (PLA) and Nylon respectively. The footplate must be set inside a shoe when using the AFO. Due to space limitations, the thickness of the footplate should be small, so the material Titanium alloy was chosen to maintain its strength. This part was made by stamping press.

This study built a computer-aid design model of the AFO using SolidWorks (D. S. Solidworks Corp., USA) and its finite element model using ANSYS® (Swanson Analysis Inc., USA). To imitate the shank, a holder was designed and bonded with the AFO cuff. The dimensions of the AFO are shown in Fig. 1(b). The footplate is set as a frame, and a sketched jig mechanism involved in the following fatigue testing platform is also disclosed. This is the initial position when the AFO was placed on the fatigue testing platform. The locations of the load cell and the point of application (PoA) were referred to the footplate. The PoA is the location where the load is applied to the AFO.

In the material of the finite element AFO model, standard PLA parameters (Young's modulus: 3.8 GPa) [15] and 3D print PLA parameters (Young's modulus: 1.26 GPa) were applied to the strut. Standard Nylon parameters (Young's modulus: 2.8 GPa) [15] and 3D print Nylon parameters (Young's modulus: 0.22 GPa) were applied to the joint part. The elastic modulus of Titanium alloy was set to 96 GPa, and stainless-steel plate was set to 200 GPa in all models.

The boundary conditions of the finite element model were set as follows: The bottom of the footplate was fixed, and the contact types among all components were bonded. However, the joint part has stoppers to constrain the plantar flexion of the AFO (Fig. 2). The stoppers contact the adjacent one when the AFO bending exceeds a certain angle. Therefore, we set the frictionless contact type between the surfaces of stoppers.

For better simulation quality, the hex dominant element is used for creating mesh model. Hex dominant meshing is a common mesh generation method in finite element analysis, primarily using hexahedral elements for three-dimensional models and incorporating tetrahedral elements when necessary. The advantages of this approach include improved accuracy due to the regularity of hexahedral elements, enhanced computational efficiency with fewer nodes, faster convergence, and ease of post-processing.

2.2. Estimation of the effective elastic modulus

This study adopted the effective elastic modulus for the material property of 3D printed components in the macroscale. We followed the ASTM D638 standard to estimate the effective elastic moduli of the 3D printed PLA and Nylon specimens. The specimens were made according to Type I specifications in the standard. The 3D printer, Apollo 1.0 (Prolink Co., Taiwan), was used to make the specimens. The nozzle had a diameter of 0.4 mm, and the thickness of each layer of the samples was 0.2 mm. The fill density was set to 100%, and the printing path was the only pattern that was arrayed in parallel but orthogonal between layers. The deposition direction was out of the biggest plane of the specimen (Fig. 3).

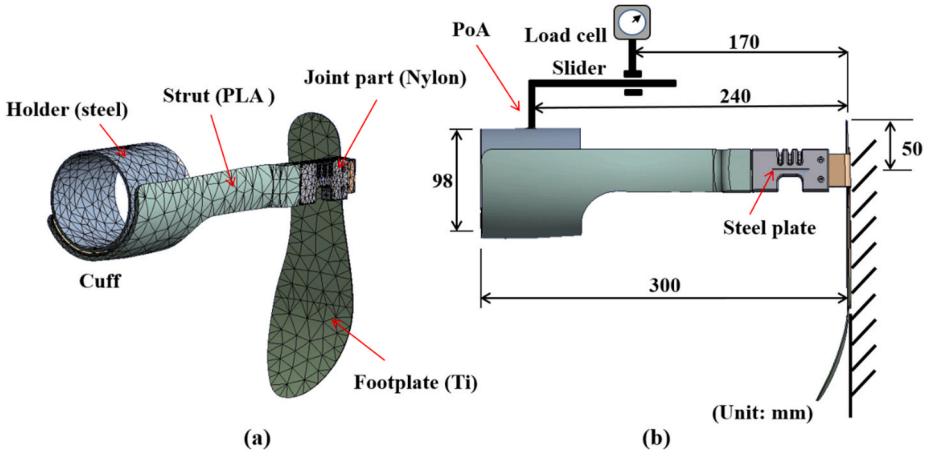

Fig. 1. (a) The computer-aid design model of the 3D printed AFO applied to the finite element simulation, and (b) the dimensions of the AFO and the position of the jig mechanism in the fatigue testing platform.

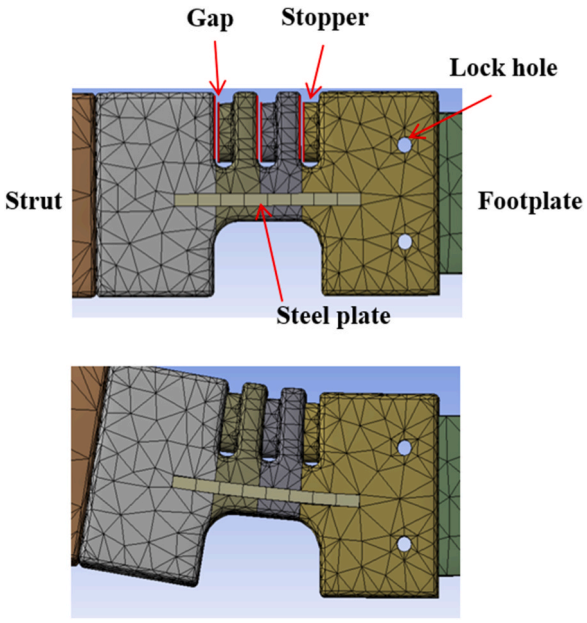

Fig. 2. The frictionless contact type between the stoppers.

We used the material testing (MT) machine, Bionix Servohydraulic Test System 370.02 (MTS System Co.), to stretch the 3D printed specimens. The deformation in the longitudinal direction was measured against the pulling force. The deformation and the pull force were transformed to the strain and stress by the known sectional area and length of the specimen. Further, the effective elastic modulus was estimated using the quasi-linear region of the curve of stress and strain. Five PLA and Nylon specimens were tested.

This study compared the effective elastic modulus of 3D printed components to that of the solid ones and also investigated how much porosity affects the effective elastic modulus. The 3D printed samples with 100% fill density were printed as cubes with a size of 30 mm. The material density of PLA and Nylon was estimated by the weight and volume of 1-m-long filaments for 3D printing. The mass of the 3D printed cube was measured and estimated by multiplying the said density and the cube volume. The porosity is the ratio of the void volume to the whole volume. It can be expressed as:

$$Porosity = \frac{V_{void}}{V_{whole}} = \left(1 - \frac{V_{real}}{V_{whole}}\right) = \left(1 - \frac{W_{real}}{W_{est}}\right) \bullet 100\% \quad (1)$$

where V_{void} the void volume, V_{whole} the whole volume, V_{real} the solid volume, W_{real} the real mass of the cube and W_{est} the estimated mass.

2.3. Fatigue testing platform

The fatigue testing platform in this study was constructed using the MT machine and the jig mechanism (Fig. 4). The jig mechanism is quite simple, and it includes a ball joint, a slider, a guide rod, and a holder. The footplate was fixed to the retaining bracket that clamped the column of the MT machine. The AFO cuff and the holder were tied together with a belt. To allow the deformation in the longitudinal axis of the shank when bending the AFO, the slider was applied. The guide rod of the slider was bonded with the holder. The ball joint was located between the load cell and the slider, and it allowed the torsion of the AFO in the transverse plane of the

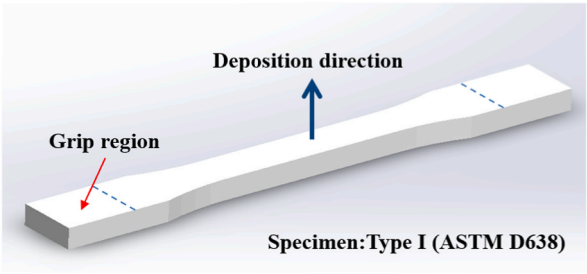

Fig. 3. The 3D printed specimens prepared for the estimation of the effective elastic modulus.

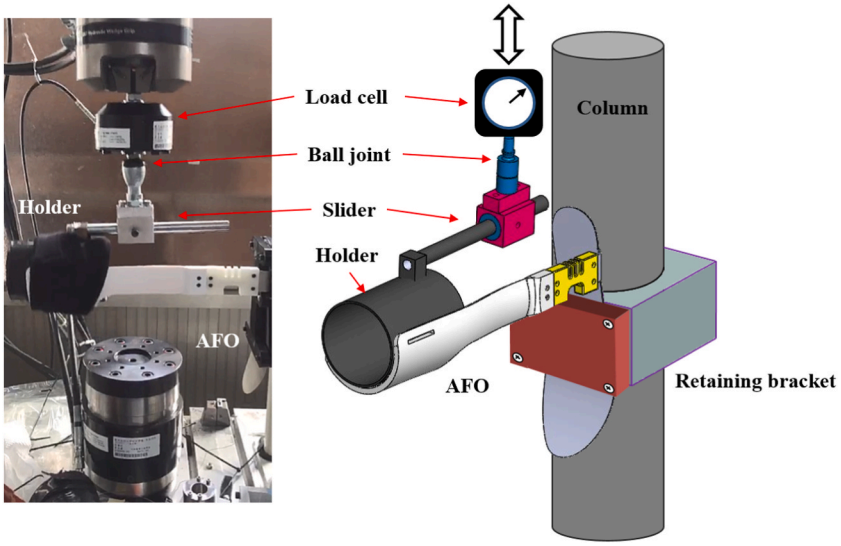

Fig. 4. The jig mechanism of the fatigue testing platform has a slider and a ball joint to tolerate the deformation of the asymmetric AFO in the fatigue test.

shank.

The PoA displacement (between −40 mm and 50 mm) used in the finite element simulation corresponds to the stroke of the MT machine, which is from −30 mm to 35 mm. The cycle time was set to 2 s, and the sampling rate was set to 5 Hz. The goal was to test each AFO for 200 thousand cycles, which is equivalent to 100 days of use if the user walks 2000 steps per day. The output parameters such as cycle count, load, displacement, and running time were measured and recorded on the computer of the MT machine.

3. Results

The effective elastic moduli of the 3D printed PLA and Nylon specimens are listed in Table 1. The elastic moduli of the solid PLA and Nylon materials (E_{ref}) are also listed [15]. When the strain was below 3.5% for PLA and below 6.5% for Nylon specimens, the functional relationship between stress and strain is quasi linear. The average of the effective elastic modulus (E_{test}) was 1.26 GPa for PLA and 0.22 GPa for Nylon. The ratio of E_{test} and E_{ref} revealed a large difference between the 3D printed and the solid components. The effective elastic modulus decreased to 1/3 for PLA and 1/12 for Nylon.

The porosity values of the 3D printed cubes are listed in Table 2. The average density of the 3D printed filaments (D_{test}) was found to be 1.32 g/cm^3 for PLA and 1.16 g/cm^3 for Nylon. The estimated mass of the PLA cube was 35.61 g, and for the Nylon cube, it was 31.67 g. The actual mass of the PLA cube (W_{real}) was measured to be 31.9 g, and for the Nylon cube, it was 26.6 g. According to Eq. (1), it can be inferred that the porosity at 100% fill density was 11% for PLA and 16% for Nylon.

To efficiently allocate limited computational resources and enhance computational efficiency in simulations, this study employs the technique of Local Mesh Refinement. This method involves using finer meshes in regions where mechanical behavior has a more pronounced impact, facilitating a more accurate capture of local variations and stress concentrations. For the mesh sensitivity study, we divide the model into critical and non-critical regions. The critical regions, including the footplate and strut, were meshed with Hex dominant elements of sizes 0.75 mm, 1 mm, 2 mm, 3 mm, 4 mm, 5 mm, and 6 mm. The remaining non-critical regions, such as the

Table 1
Effective elastic moduli of PLA and Nylon specimens.

Material	E_{test} (GPa)		E_{ref} (GPa)	Ratio (E_{test}/E_{ref})
PLA	Trail 1	1.29	3.80	0.33
	Trail 2	1.28		
	Trail 3	1.27		
	Trail 4	1.21		
	Trail 5	1.25		
	Average	**1.26**		
Nylon	Trail 1	0.21	2.80	0.08
	Trail 2	0.21		
	Trail 3	0.23		
	Trail 4	0.23		
	Trail 5	0.21		
	Average	**0.22**		

Table 2
The porosity of 3D printed PLA and Nylon cube of 27 cm^3 volume.

Material	D_{test} (g/cm^3)		W_{est} (g)	W_{real} (g)	Porosity (100% fill density)
PLA	Trail 1	1.32	35.61	31.90	11%
	Trail 2	1.32			
	Trail 3	1.32			
	Average	**1.32**			
Nylon	Trail 1	1.17	31.67	26.60	16%
	Trail 2	1.17			
	Trail 3	1.13			
	Average	**1.16**			

stainless-steel plate and joint part, were meshed using a 5 mm Hex dominant element size. With applying a 15 mm plantarflexion movements displacement at the cuff, stress indicators at the center point of the stainless-steel plate were observed. The results show that the mesh in the non-critical regions converged when the element size was reduced to below 2 mm (with error less than 5%). Therefore, this study adopts a Hex dominant element size of 2 mm for subsequent finite element model meshing (Table 3).

To investigate kinetic responses such as the load, bending resistance, equivalent stress, and regions of stress concentration, The models were subjected to simulated dorsiflexion and plantarflexion movements with 50 mm displacement at the cuff. The loadings were applied to two models with different material set. Standard material model uses standard PLA and standard Nylon materials, 3D print material model use 3D print PLA and 3D print Nylon.

The results shows that the maximum equivalent stress occurred on the steel plate. The values for standard material set were dorsiflexion: 845.16 MPa (Fig. 5(a)), and plantarflexion: 839.54 MPa (Fig. 5(c)), and for 3D print material set were dorsiflexion: 523.81 MPa (Fig. 5(b)) and plantarflexion: 497.73 MPa (Fig. 5(d)). The maximum equivalent elastic strain occurred on the joint part. The values for the standard material set were dorsiflexion: 3.48% (Fig. 6(a)) and plantarflexion: 9.93% (Fig. 6(c)), and for the 3D print material set were dorsiflexion: 3.58% (Fig. 6(b)) and plantarflexion: 8.95% (Fig. 6(d)). Additionally, the forces sustained by the stopper structure on the joint part changed due to the different models and loading patterns. In the simulation of dorsiflexion, the force on the stopper structure was 0. In the simulation of plantarflexion, the forces on the three stopper structures are, in the standard material set, 26.65 N, 15.34 N, and 6.4 N, and in the 3D print material set, 70.16 N, 55.15 N, and 66.48 N, respectively.

This study obtained the loads of the 3D printed and solid AFOs by varying the PoA displacement in the simulation. The loads are shown in (Fig. 7), where positive displacement corresponds to plantar flexion and negative displacement corresponds to dorsiflexion. The slope of the curve represents the stiffness of the AFO, and both slopes increase noticeably when the displacement is more than 30 mm. This is because the stoppers start to contact each other, and the stiffness of the AFO or bending resistance grows as a result. The increased resistance helps prevent drop foot in patients with stroke [16]. The stiffness of the 3D printed AFO is about 1/5 of the solid AFOs.

The stroke of the MT machine is proportional to the PoA displacement, and the load and displacement of the load cell can be evaluated using PoA. Therefore, the loads in the simulation can be compared with the experimental data of the load cell. The data are shown in (Fig. 8). No obvious damage was observed on the 3D printed AFO during the fatigue test. The applied load varied between −21 N and 34 N, and it increased significantly once the stroke exceeded 20 mm, causing the stoppers start to contact each other. A PoA displacement of 30 mm corresponds to a stroke of 21 mm on the stroke scale.

4. Discussion

This study used the FDM technology to produce the AFO components. This 3D printed components are porous and anisotropic. The ASTM D638 standard provided a way to estimate the effective elastic modulus of 3D printed component. The effective elastic modulus was much smaller than that of the solid material. The porosity of 3D printed cubes at 100% fill density is not zero, which is 11% for the PLA and 16% for Nylon in this study. The porosity significantly affected the effective elastic modulus. Thus, the 3D printed components at 100% fill density should not be considered as solid material in the finite element simulation. For research adopting lower fill densities, the effective elastic modulus of each 3D printed specimen with different fill density and patterns should be measured first to set the material properties in the simulation. Furthermore, a lookup table can be built to determine the effective elastic modulus based

Table 3
Mesh sensitivity study.

Model No.	Element size of critical regions	Nodes	Elements	von Mises stress at center of the steel plate	Max principal strain at steel plate	Min principal strain at steel plate
1	0.75 mm	391742	106450	140.17	0.000784	−0.000774
2	1 mm	192342	52766	137.69	0.000771	−0.000761
3	2 mm	74654	22298	133.38	0.000744	−0.000736
4	3 mm	48342	14909	145.58	0.000858	−0.000862
5	4 mm	42439	13024	114.77	0.000709	−0.000692
6	5 mm	39815	12241	103.63	0.000498	−0.000459
7	6 mm	38693	12023	83.09	0.000487	−0.000452

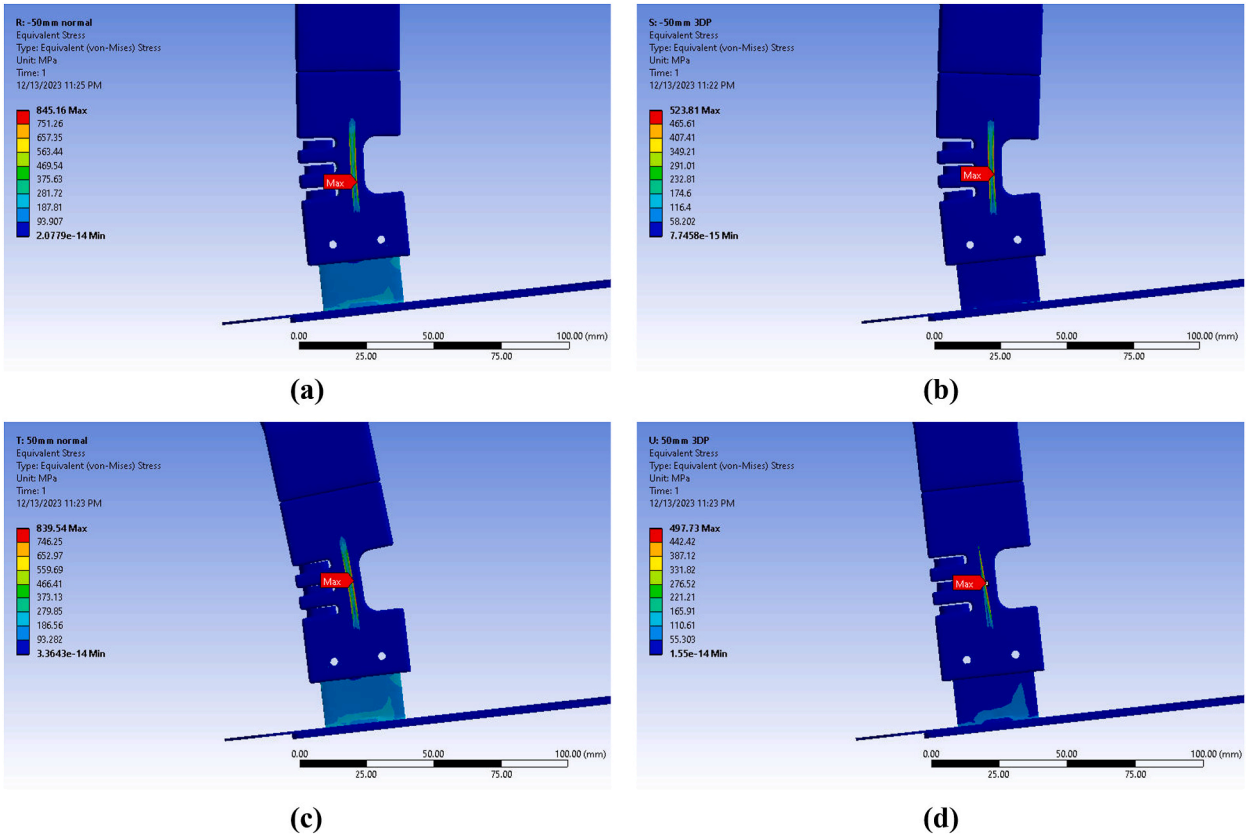

Fig. 5. The maximum equivalent stress observed in the steel plate area of the joint part: (a) dorsiflexion simulated with standard material parameters, (b) dorsiflexion simulated with 3D print material parameters, (c) plantar flexion simulated with standard material parameters, and (d) plantar flexion simulated with 3D print material parameters.

on the fill density and printing patterns. This study also investigated the difference of the porosity between PLA and Nylon. We used the same printing parameters to make the cubes, and the porosity of PLA and Nylon cubes should not be different. The difference may come from the higher shrinkage rate of Nylon compared to that of PLA, which is why we found the porosity of the Nylon cube to be higher.

The strength is affected by the printing path pattern and fill density, and lower fill densities can result in shorter manufacturing times but weaker components. Yeh et al. [17] found that concentric patterns have weaker torsion resistance than other patterns at fill densities below 100%. To increase the strength of FDM components, researchers have developed methods such as using wavy printing paths to enhance strength and aligning alternating layups symmetrically with respect to the loading direction to increase toughness [18]. Kuznetsov et al. [19] discovered that decreasing the layer thickness and increasing the nozzle size resulted in higher strength of the 3D printed structure. Kiendl et al. [20] aligned the alternating layups symmetrically with respect to the loading direction for the FDM process to increase the toughness of 3D printed samples. These FDM-related researches provided ways to strengthen the 3D printed components when the fill density was lower than 100%. This study doesn't consider the fill density is lower than 100%, and thereby only one patten with the aligning alternating layups could be used. Based on the same geometric profile, the solid material has higher strength than the porous one. Besides, the 3D-printed structure in FDM is anisotropic, it is more obvious when the fill density is lower than 100% because of the various patterns. It is weak against the torsion. Thus, AFO was supposed to be a solid and homogenous structure. For the 3D-printed AFO, Increasing the fill density appears to be a better way to strengthen.

In the fatigue test, 200 thousand cycles are equivalent to 100 days of usage assuming the user walks 2000 steps per day. Cha et al. [12] also conducted fatigue tests on their 3D printed AFO, which had a lifespan of 120 days. Improving the lifespan of 3D printed AFOs can be helpful in reducing the cost burden. High stress concentration can lead to destruction, particularly after long-term use. In this study, the metal plate bears most of the load in the joint part, where stress concentration occurs, making it the most vulnerable part of the AFO. To extend the lifespan of the AFO, a tougher type of metal or a thicker plate is recommended. Additionally, the metal plate should be designed for easy replacement and maintenance. The bend portion of the footplate also undergoes stress concentration due to its high curvature. Using a better-rounded corner or a longer arch is also recommended. The estimation of the effective elastic modulus was based on the quasi-linear relationship between the stress and strain. However, some portions of the joint part had a maximum of 8.5% strain. Even if this leads to plastic deformation, the small affected regions could be ignored, as evidenced by the fact that the joint part did not deform noticeably after the fatigue testing.

The simulation data approximates the experimental data in (Fig. 8), and thus the finite element model is reliable. If the 3D printed

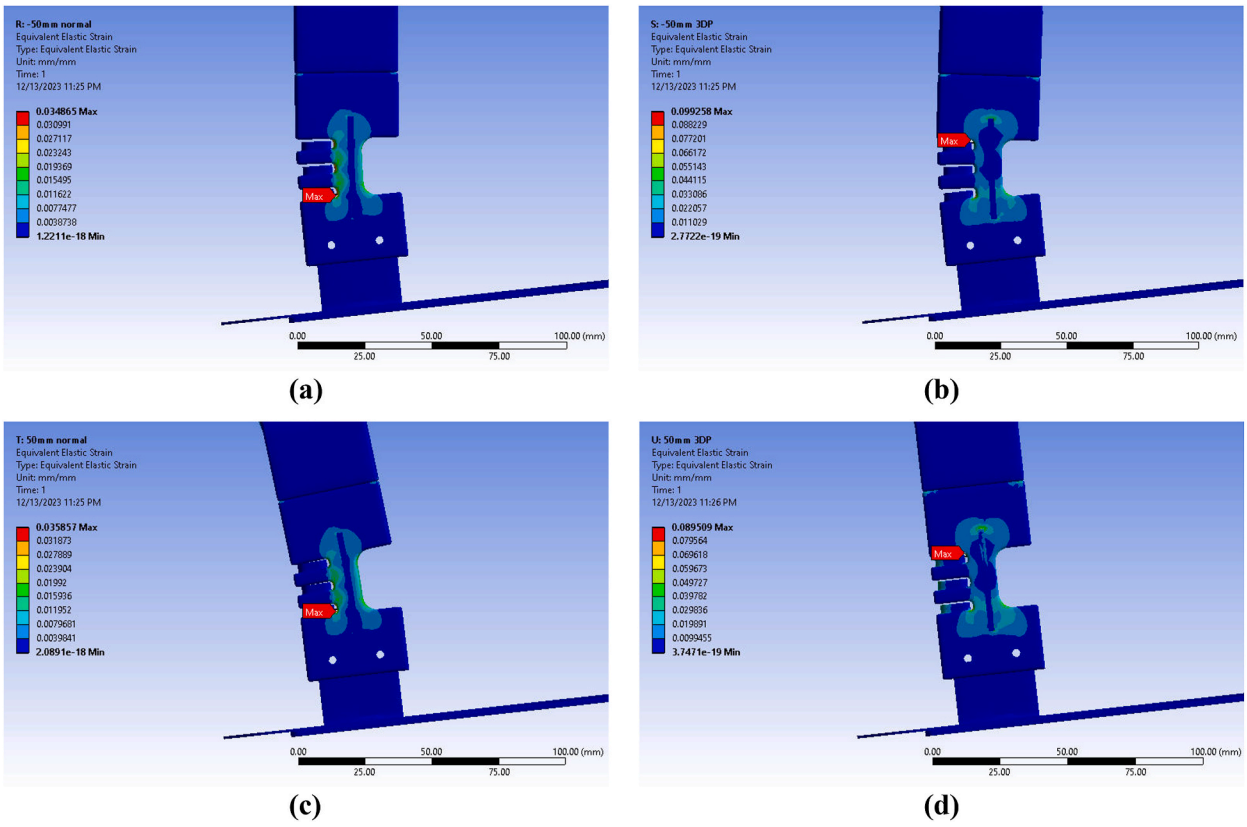

Fig. 6. The maximum strain occurred in the joint part: (a) dorsiflexion with standard material parameters, (b) dorsiflexion with 3D print material parameters, (c) plantar flexion with standard material parameters, and (d) plantar flexion with 3D print material parameters.

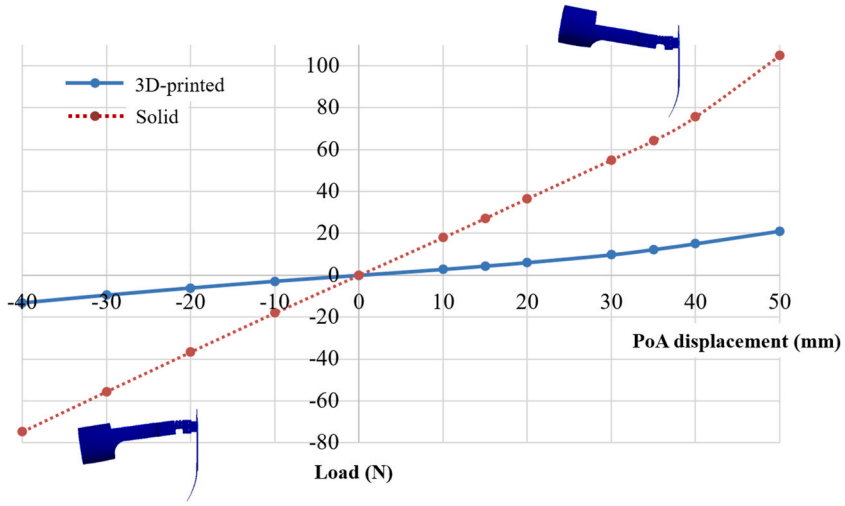

Fig. 7. The comparison of the loads of 3D printed and solid AFOs in the finite element simulation.

AFO is designed using the finite element model with solid material properties, the product will be more flexible because the effective elastic modulus of 3D printed components is lower. The stiffness of the AFO affects the resistance for preventing drop foot and the stability in walking. To achieve the suitable stiffness, the designer of the 3D printed AFO needs a precise finite element model to obtain the true kinetic features. Previous studies have used finite element method to investigate the stress distribution in AFOs [21,22]. Marsalek et al. [23] utilized finite element analysis as a replacement for physical testing of 3D printed cranial orthoses. Finite element analysis was also used in the simulation of conventional and articulated 3D printed AFOs [24]. Our study adopted the effective elastic

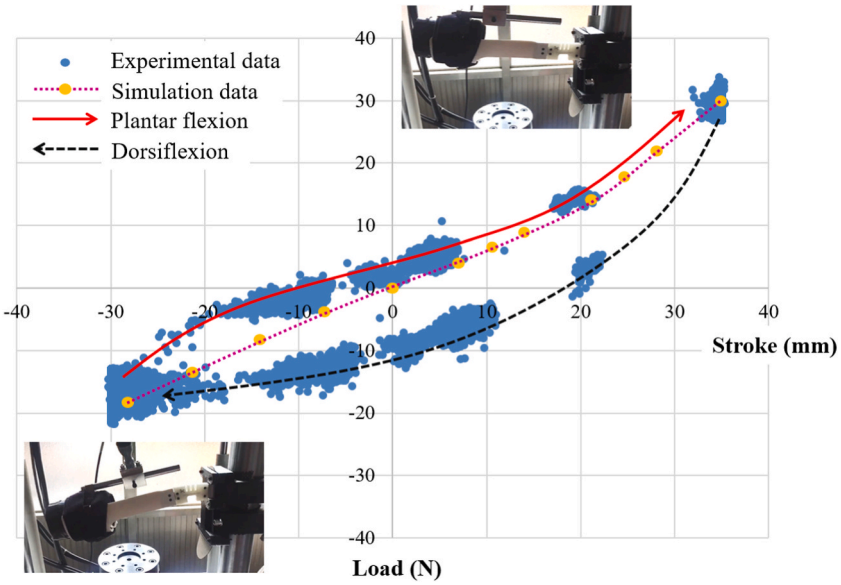

Fig. 8. The finite element model can match the experimental data of the fatigue test.

modulus to correct the finite element model of the 3D printed AFO, and the fatigue testing platform verified the feasibility of the model. To the best of our knowledge, this is the first article to emphasize the significance of calculating the effective elastic modulus to determine the actual porosity of 3D printed samples, which allows for more precise finite element simulation. This study provides valuable insights into the production and optimization of 3D printed AFOs for patients with stroke.

On the other hand, some research has focused on establishing the actual 3D printed structures. Zarbakhsh et al. [25] created a sub-model finite element analysis for the porous structure and found that stress concentration appears between the layers. The method reveals a detailed simulation, but building plenty of finite element models for 3D printed components with different fill densities and printing patterns is complicated. Both models provide a more accurate simulation for 3D printed samples. However, material testing of specimens or the sub-modeling approach is necessary in advance. Obtaining effective mechanical properties is simpler and more convenient than making sub-modeling structures for AFOs.

The jig mechanism of the fatigue testing platform was designed to allow the deformation of the AFO between dorsiflexion and plantar flexion. Other studies [7,12–14] used symmetric AFOs, which have only one strut located behind the shank or two struts located by the ankle joint, and their measuring platforms only work in the sagittal plane. Our fatigue testing platform allows deformation not only in the sagittal plane but also in the transverse plane of the shank. Some asymmetric AFOs, such as our AFO and the ToeOFF (Allard Int.), are applicable to our fatigue testing platform, but our platform cannot measure the torque of the asymmetric AFOs in the transverse plane. The larger plantar flexion or dorsiflexion has a larger torque that affects the abduction and adduction of the foot. The designer of an asymmetric AFO should consider the torque effect in a gait cycle. Therefore, an advanced fatigue testing platform will install a torque sensor, and the bonded ways of wearing the AFO or the stability of the AFO in walk can be further discussed and improved.

It is worth noting that the findings of this study have been further investigated in a clinical trial. Our specialized 3D printed AFO has been shown to enhance gait performance and satisfaction when compared to the traditional anterior AFO [16]. However, this study still has its limitations. As shown in (Fig. 8), the simulation results closely matched the experimental findings, where the red solid line represents plantar flexion load and the black dashed line represents dorsiflexion load. Both lines exhibited a hysteresis effect attributed to the viscoelastic properties of the material. Nevertheless, this study did not incorporate the hysteresis effect into the simulation. The finite element models has limitation as well. While the computer model closely resembles the 3D print model in geometric shape, the use of FDM in the print process introduces disparities with homogeneous isotropic materials. Future research needs to explore improved methodologies for finite element simulations of 3D printing. Discrepancies in boundary condition settings between finite element simulations and mechanical experiments may lead to result inaccuracies. Additionally, the simplification of physical connections, represented as bonding in the computer model, introduces potential numerical deviations that can impact simulation accuracy.

5. Conclusion

This study utilized the effective elastic modulus to adjust the finite element model of the 3D printed AFO. The porosity of 3D printed components is not zero even when the fill density is set to 100% during the FDM process. This porosity affects the effective elastic modulus of the 3D printed component, and therefore the estimation of the effective elastic modulus should be performed for components with different fill densities and printing patterns. The fatigue testing platform confirmed the feasibility of the finite element

model. Furthermore, the fatigue testing platform is suitable for testing asymmetric AFOs since it allows for deformation in both the sagittal and transverse planes of the shank.

Funding

This study was supported by the Ministry of Science and Technology of Taiwan (Grant no. MOST107-2218-E006-010) and National Science and Technology Council (NSTC112-2221-E−214-017), as well as Ministry of Education, Taiwan.

Ethical approval

Not required.

CRediT authorship contribution statement

Chien-Hsien Yeh: Writing – original draft, Investigation, Data curation, Conceptualization. **Keng-Ren Lin:** Writing – review & editing, Methodology, Formal analysis, Data curation. **Fong-Chin Su:** Supervision. **Hsiu-Yun Hsu:** Supervision. **Li-Chieh Kuo:** Supervision, Methodology. **Chih-Chun Lin:** Writing – review & editing, Writing – original draft, Funding acquisition, Conceptualization.

Declaration of competing interest

The authors declare no competing interests.

Acknowledgments

This work was supported by the Medical Device Innovation Center (MDIC), National Cheng Kung University (NCKU) from the Featured Areas Research Center Program within the framework of the Higher Education Sprout Project of the Ministry of Education in Taiwan.

Appendix A. Supplementary data

Supplementary data to this article can be found online at https://doi.org/10.1016/j.heliyon.2024.e26926.

References

[1] K. Pongpipatpaiboon, et al., The impact of ankle-foot orthoses on toe clearance strategy in hemiparetic gait: a cross-sectional study, J. NeuroEng. Rehabil. 15 (1) (2018) 41.
[2] F. Gao, W. Carlton, S. Kapp, Effects of joint alignment and type on mechanical properties of thermoplastic articulated ankle-foot orthosis, Prosthet. Orthot. Int. 35 (2) (2011) 181–189.
[3] B. Neubauer, W. Durfee, Preliminary design and engineering evaluation of a hydraulic ankle–foot orthosis, J. Med. Dev. Trans. ASME 10 (4) (2016).
[4] C. Mavroidis, et al., Patient specific ankle-foot orthoses using rapid prototyping, J. NeuroEng. Rehabil. 8 (1) (2011) 1.
[5] M. Walbran, K. Turner, A.J. McDaid, Customized 3D printed ankle-foot orthosis with adaptable carbon fibre composite spring joint, Cogent Eng. 3 (1) (2016).
[6] S. Telfer, et al., Embracing additive manufacture: implications for foot and ankle orthosis design, BMC Muscoskel. Disord. 13 (1) (2012) 84.
[7] E.S. Schrank, et al., Assessment of a virtual functional prototyping process for the rapid manufacture of passive-dynamic ankle-foot orthoses, J. Biomech. Eng. 135 (10) (2013) 101011–101017.
[8] X. Wang, et al., Effect of porosity on mechanical properties of 3D printed polymers: experiments and micromechanical modeling based on X-ray computed tomography analysis, Polymers 11 (7) (2019) 1154.
[9] D.W. Abbot, et al., Finite element analysis of 3D printed model via compression tests, Procedia Manuf. 35 (2019) 164–173.
[10] J. Kováčik, Correlation between Young's modulus and porosity in porous materials, J. Mater. Sci. Lett. 18 (13) (1999) 1007–1010.
[11] H.J. Lai, et al., Ankle-foot simulator development for testing ankle-foot orthoses, Med. Eng. Phys. 32 (6) (2010) 623–629.
[12] Y.H. Cha, et al., Ankle-foot orthosis made by 3D printing technique and automated design software, Appl. Bionics Biomech. 2017 (2017) 9610468.
[13] D.J.J. Bregman, et al., A new method for evaluating ankle foot orthosis characteristics: bruce, Gait Posture 30 (2) (2009) 144–149.
[14] T. Kobayashi, et al., Design of an automated device to measure sagittal plane stiffness of an articulated ankle-foot orthosis, Prosthet. Orthot. Int. 34 (4) (2010) 439–448.
[15] G.A. Johnson, J.J. French, Evaluation of infill effect on mechanical properties of consumer 3D printing materials, Adv. technol. innov. 3 (4) (2018) 179–184.
[16] C.-C. Lin, et al., Evidence-based customized ankle-foot orthosis with energy storage, J. Med. Biol. Eng. 41 (2) (2021) 126–136.
[17] C.-H. Yeh, et al., Mechanical problem in 3D printed ankle-foot orthoses with function of energy storage, AIP Conf. Proc. 2046 (1) (2018) 020019.
[18] Y. Jin, Y. He, A. Shih, Process planning for the fuse deposition modeling of ankle-foot-othoses, Procedia CIRP 42 (2016) 760–765.
[19] V.E. Kuznetsov, et al., Strength of PLA components fabricated with fused deposition technology using a desktop 3D printer as a function of geometrical parameters of the process, Polymers 10 (2018), https://doi.org/10.3390/polym10030313.
[20] J. Kiendl, C. Gao, Controlling toughness and strength of FDM 3D-printed PLA components through the raster layup, Compos. B Eng. 180 (2020) 107562.
[21] R. Raj, et al., Numerical and experimental mechanical analysis of additively manufactured ankle-foot orthoses, Materials 15 (17) (2022).
[22] T.M. Chu, N.P. Reddy, J. Padovan, Three-dimensional finite element stress analysis of the polypropylene, ankle-foot orthosis: static analysis, Med. Eng. Phys. 17 (5) (1995) 372–379.

[23] P. Marsalek, et al., Virtual prototyping of 3D printed cranial orthoses by finite element analysis, AIP Conf. Proc. 2116 (1) (2019) 320010.
[24] M.H. Ali, Z. Smagulov, T. Otepbergenov, Finite element analysis of the CFRP-based 3D printed ankle-foot orthosis, Proc. Comput. Sci. 179 (2021) 55–62.
[25] J. Zarbakhsh, A. Iravani, Z. Amin-Akhlaghi, Sub-modeling finite element analysis of 3D printed structures, in: 2015 16th International Conference on Thermal, Mechanical and Multi-Physics Simulation and Experiments in Microelectronics and Microsystems, 2015, pp. 1–4.